ACS Photonics

pubs.acs.org/journal/apchd5 Article

Large Numerical Aperture Metalens with High Modulation Transfer Function

Jian Zhang, Xiong Dun,* Jingyuan Zhu, Zhanyi Zhang, Chao Feng, Zhanshan Wang, Wolfgang Heidrich, and Xinbin Cheng*

Cite This: https://doi.org/10.1021/acsphotonics.2c02029 Read Online

ACCESS | Metrics & More | Article Recommendations | Supporting Information

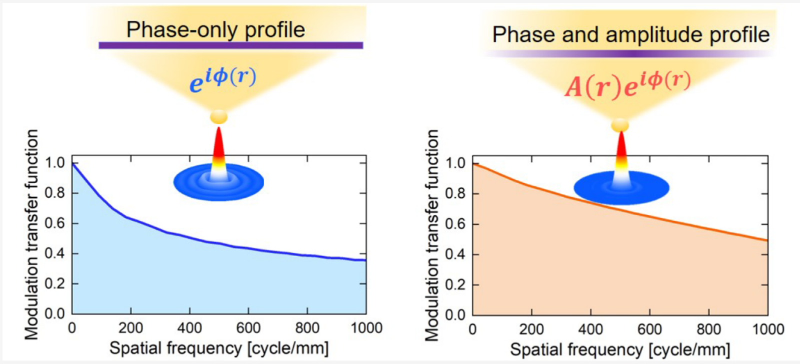

ABSTRACT: Large numerical aperture (NA) lenses with high modulation transfer functions (MTFs) promise high image resolution for advanced optical imaging. However, it is challenging to achieve a high MTF using traditional large-NA lenses, which are fundamentally limited by the amplitude mismatch. In contrast, metasurfaces are promising for realizing amplitude and phase matching for ideal lenses. However, current metalenses are mostly based on a phase-only (PO) profile because the strong coupling among the metaatoms in large-NA lenses makes perfect amplitude matching quite challenging to realize. Here, we derive a phase-and-amplitude (PA) profile that approaches the theoretical MTF limit for large-NA lenses and use interferometric unit cells combined with a segmented sampling approach to achieve the desired amplitude and phase control. For the first time, we show that the amplitude does not require a perfect match; realizing the trend of the required amplitude is sufficient to significantly increase the MTF of a large-NA lens. We demonstrated a 0.9 NA cylindrical metalens at 940 nm with a Struve ratio (SR), which describes how close the MTF is to the upper limit, increasing from 0.68 to 0.90 compared with the PO metalens. Experimentally, we achieved an SR of 0.77 for the 0.9 NA lens, which is even 0.09 higher than the simulated SR of the PO metalens. Our investigation provides new insights for large-NA lenses and has potential applications in high-image-resolution optical systems.

KEYWORDS: *large numerical aperture, metalens, amplitude, phase, high modulation transfer function*

■ INTRODUCTION

High-resolution optical systems, such as cylindrical lenses for line illumination microscopy[1] and compound lenses for confocal scanning microscopy,[2,3] are essential to advanced imaging. Attaining high resolution requires large numerical aperture (NA) lenses with high modulation transfer functions (MTFs), because the NA determines the theoretical resolution limit of the optical system[4,5] and the MTF reflects the attained resolution.[4,6,7] Alù et al.[8] and Di et al.[9] have rigorously analyzed that achieving a high MTF at a large NA requires the co-modulation of the phase and amplitude. Traditional refractive and diffractive lenses[10−12] generally modulate the light phase, resulting in an increase in the side-lobe energy of focus for large-NA lenses. Consequently, as the NA increases, they suffer a significant drop in the MTF compared to the upper limit determined by a perfect lens. This drop in performance can be characterized by the Struve ratio (SR),[7] which quantitatively reflects the closeness of the MTF to the theoretical limit (the larger the SR value, the higher the MTF). Some techniques, such as aperture apodization,[13,14] allow reducing the side lobes in refractive lenses through amplitude modulation, but at the cost of increased system complexity and some loss in resolution.[13]

Metasurfaces, a novel artificial material composed of subwavelength structures, offer a significant ability to modulate

Received: December 30, 2022

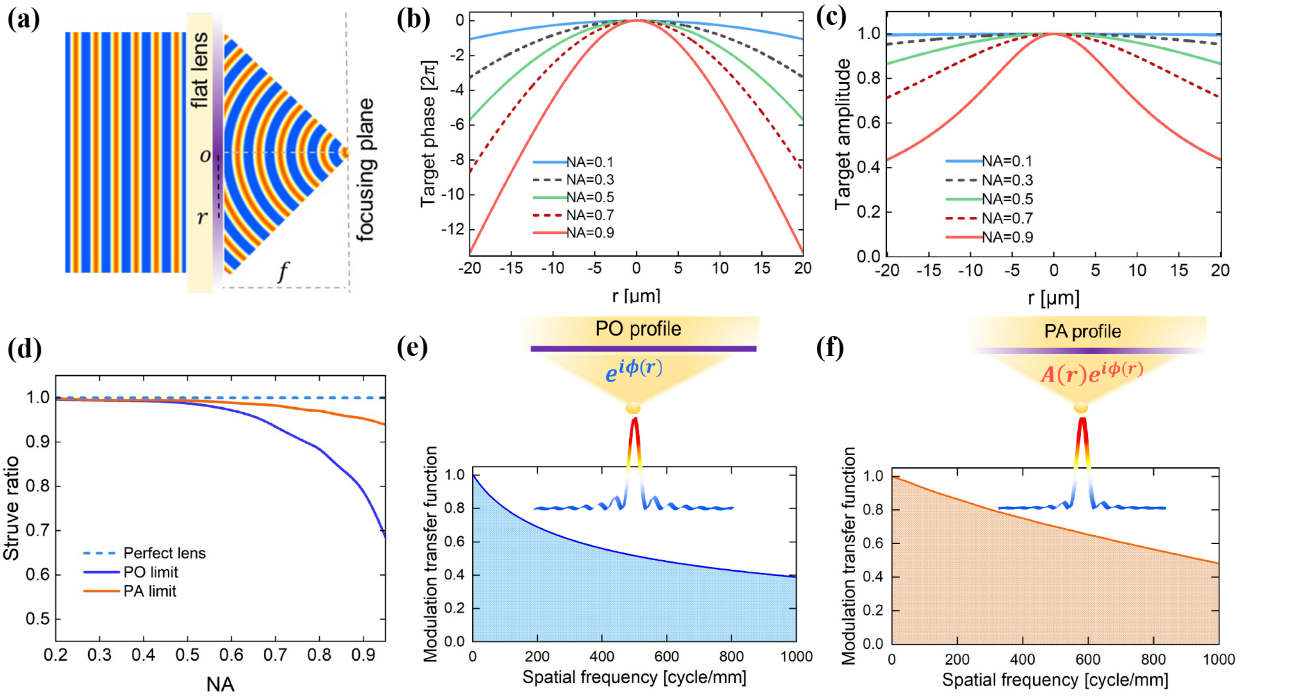

Figure 1. Illustration of the phase-and-amplitude (PA) profile and its effect. (a) Schematic diagram of a perfect flat lens. View from right to left is a point source of radiation. The purple gradient line represents the various amplitude and phase distributions when the spherical wave radiates to the flat plane. (b, c) Phase and amplitude distributions for different NAs according to the PA profile. (d) Ideal SR for the cylindrical lens designed with phase-only (PO) and PA profiles and 0.2−0.95 NAs. (e, f) The virtual lenses with 0.9 NA created by the PO and PA profiles exhibit increased and decreased side lobes, respectively.

both the amplitude and phase of light[15−20] and promise to realize large-NA imaging devices with high MTFs. However, particularly for a large NA, it is difficult to directly design metalenses that achieve the rigorous amplitude and phase matching requirement given by refs 8 and 9 because of the strong electromagnetic coupling between adjacent unit cells. Thus, several pioneering studies on large-NA metalenses[21−27] did not consider the amplitude requirement, usually basing their designed metalenses on the phase-only (PO) profile proposed by ref 28 and resulting in a dramatically decreasing MTF with an increasing NA.[9] Some inverse design methods, such as topology optimization,[9,29−31] do not apply the phase-only constraint and directly optimize the subwavelength structure to design large-NA metalenses. Although this could be a solution, it has several limitations. First, optimization relies heavily on a good heuristic initial design that serves as a starting point. Second, inverse design requires enormous computational resources that exponentially grow with the device size,[26] which leads to poor scalability (limits the size of the device). Moreover, it is difficult to fabricate an optimized free structure. Therefore, a large-NA (e.g., NA = 0.9) metalens that approaches the theoretical MTF limit has not yet been experimentally demonstrated.

In this study, to improve the MTF, we find that the amplitude of a large-NA lens does not require perfect matching; it suffices to realize approximately the trend of the required amplitude. Specifically, by investigating the radiation field of a point source, we first propose a simplified phase and amplitude matching requirement, the phase-and-amplitude (PA) profile, which allows metalenses to approach the upper limit of the MTF of a large-NA lens. Then, we use interferometric unit cells that modulate the amplitude and phase independently and adopt a segmented sampling principle to construct the metalens. As a proof of concept, we design a 0.9 NA cylindrical PA metalens illuminated by 940 nm TE-polarized light. Although the actual amplitude of the metalens does not perfectly fit the target amplitude (it oscillates along the target to some extent), it nevertheless achieves an SR of 0.90, which is a marked improvement over the respective SR of 0.68 of a counterpart PO design. Furthermore, the SR of our 0.9 NA design is higher than the highest theoretically achievable SR of phase-only designs. Finally, we fabricated and characterized the proposed 0.9 NA cylindrical metalens and experimentally demonstrated that its SR was 0.77, which was higher than the simulated SR of the PO metalens, thus confirming our findings.

■ RESULTS

PA Profile for a Large-NA Lens with High MTF. We derived the PA profile from the standpoint of a radiating point source by analyzing the amplitude and phase distribution of the point source placed at the focus point that propagates back to the surface of the lens via optical reciprocity. Figure 1(a) shows a plane wave focused into an ideal spot through a flat lens; according to the scalar spherical wave approximation,[5,32,33] the complex amplitude of the wave radiated by the point light source at the lens plane is $Ae^{ik(\sqrt{r^2+f^2})}/\sqrt{r^2+f^2}$, where f is the focal length of the flat lens, $k = 2\pi/\lambda$ is the wavenumber, r is the distance from the center of the lens, and A is the intensity of the point source. The amplitude of the radiated wave on the flat plane gradually decreases from the center to the edge. Conversely, to convert a normal incident plane wave with an amplitude of unity into an ideal spherical wave, a flat lens (metalens) must achieve the following complex amplitude modulation:

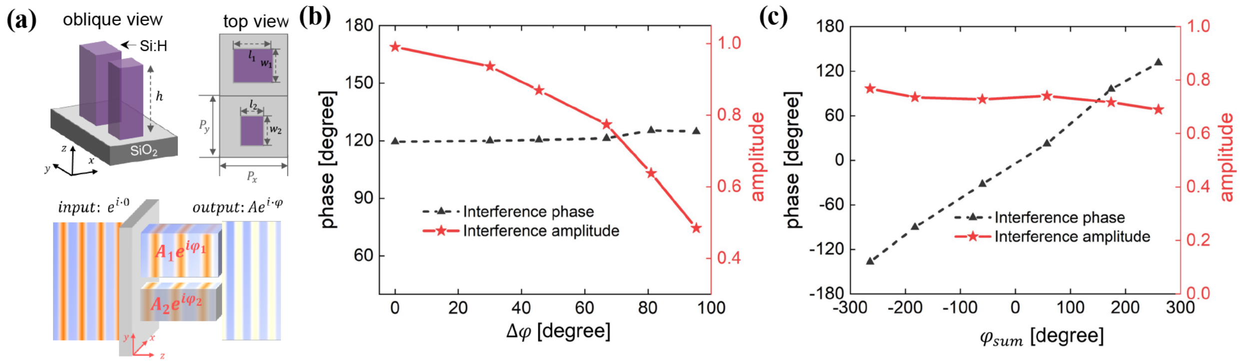

Figure 2. Illustration of interferometric unit cells and the amplitude and phase modulation results. (a) Schematic diagram of interferometric unit cells composed of two substructures in the same period. The substructure dimension (l, w) can be changed to provide the desired propagation phase. The bottom is a schematic illustration of a plane wave turning into waves of independent amplitudes and phases via the interferometric unit cell. (b) While fixing the phase at $\varphi_{\text{sum}} = 240°$, the amplitude is adjusted by changing the phase difference $\Delta\varphi$ from 0° to 95°. (c) The phase is changed through the phase summation φ_{sum} from −260° to 260° when the phase difference $\Delta\varphi$ is −80°.

$$t_{\text{flatlens}} = A_0 \frac{f}{\sqrt{r^2 + f^2}} \exp[-ik(\sqrt{r^2 + f^2} - f)] \tag{1}$$

where A_0 represents the amplitude at the center of the lens. Regarding maintaining energy conservation, A_0 needs to be larger than 1 (see Supporting Information for details). So, the lens needs to transfer excess energy from the border to the center, which is challenging. To be more feasible, we ignore the energy conservation and take A_0 as 1 to only achieve the relative amplitude. Most importantly, although some excess energy is lost, the transmitted light remains an ideal spherical wave and does not affect the MTF or imaging quality.[7]

Figure 1(b) and (c) illustrate the phase and amplitude distributions of the various NAs. It can be seen that the phase is still a hyperbolic phase, but the amplitude is no longer unity as the NA increases. When the NA is less than 0.5, the amplitude remains almost unchanged; therefore, the ideal SR of the cylindrical lens design with a PO profile is close to 1, as shown in Figure 1(d). Once the NA exceeds 0.5, the amplitude varies significantly across the aperture; consequently, the ideal SR of the PO design decreases rapidly. For example, the ideal SR of the lens design with the PO profile drops to 0.8 when the NA reaches 0.9. By adding the proposed amplitude modulation instead of a uniform amplitude, the PA profile improves the ideal SR, as indicated by the orange line in Figure 1(d). With the same 0.9 NA, an SR of 0.96 can theoretically be achieved with the PA profile. Note that because of the scalar approximation, there remains a 0.04 difference between perfect lenses; however, our PA profile improves the ideal SR by 0.16 compared to that of the PO profile. As shown in Figure 1(e) and (f), this improvement is due to the PA profile decreasing the side-lobe energy of the point-spread function (PSF) to make the energy more concentrated and hence enhances the MTF. Please refer to the Supporting Information for more details on the calculation of MTFs and SRs.

Design of a Large-NA and High-MTF Metalens. The proposed PA profile shows the amplitude and phase profile requirements for large-NA lenses with a high MTF. In this section, we utilize interferometric unit cells that can achieve independent amplitude and phase modulations to design and realize these profiles.

Interferometric Unit Cells. Traditional unit cells[24] are unsuitable for constructing PA metalenses because they cannot independently modulate amplitude and phase. However, two emergent kinds of unit cells have such ability; one is the unit cell based on the conversion efficiency of circularly polarized light,[34−36] and the other is the interferometric unit cell[37−40] with multiple metaatoms. The latter has higher energy utilization efficiency and more structural degrees of freedom than the former. Therefore, we chose interferometric unit cells to design metalens. The structure of the interferometric unit cell is shown in Figure 2(a). The interferometric unit cell is composed of two substructures with the same period arranged along the y axis. When the plane wave $e^{i\cdot 0}$ is incident, the electric field distributions of the two substructures can be expressed as $A_1e^{i\cdot\varphi_1}$ and $A_2e^{i\cdot\varphi_2}$. The interference occurs near the output surface of the unit cells owing to the subwavelength separation of the substructures. The average interference complex amplitude is given by $Ae^{i\cdot\varphi} = (A_1e^{i\cdot\varphi_1} + A_2e^{i\cdot\varphi_2})/2$. For the high-transmittance subunit cells, where A_1 and A_2 are close to 1, the resultant amplitude and phase can be simplified as

$$A = \frac{1}{2}\sqrt{2 + 2\cos(\Delta\varphi)}, \qquad \varphi = \frac{\varphi_{\text{sum}}}{2} \tag{2}$$

where $\Delta\varphi = \varphi_1 - \varphi_2$ and $\varphi_{\text{sum}} = \varphi_1 + \varphi_2$. Please refer to the Supporting Information for derivation details.

According to eq 2, the amplitude modulation generated by the interferometric unit cells is dependent only on $\Delta\varphi$, and their phase modulation is dependent only on φ_{sum}. Note $\Delta\varphi$ and φ_{sum} are linearly independent, so we can independently modulate the amplitude A and phase φ. Figure 2(b) shows an example that when keeping φ_{sum} to 240° to retain the phase φ at 120°, the amplitude A can be adjusted individually by altering the phase difference $\Delta\varphi$. Similarly, Figure 2(c) shows an example in which $\Delta\varphi \cong -80°$ to retain amplitude A at 0.75. The phase φ is changed individually by altering the phase summation φ_{sum}. See the Supporting Information for the modulation approach of the phase summation (difference) and additional examples of independent modulation of the phase and amplitude. Controlling coupling is a crucial factor in designing interferometric unit cells; in this paper, we choose a high refractive index hydrogenated silicon (Si:H) material (n = 3.49, k = 0.001)[41] because it can enhance the structure's ability to confine the electric field and reduce the coupling.[41−43] Although the extinction coefficient k of Si:H is not very small, it has little effect on the metalens (see the Supporting

https://doi.org/10.1021/acsphotonics.2c02029
ACS Photonics XXXX, XXX, XXX−XXX

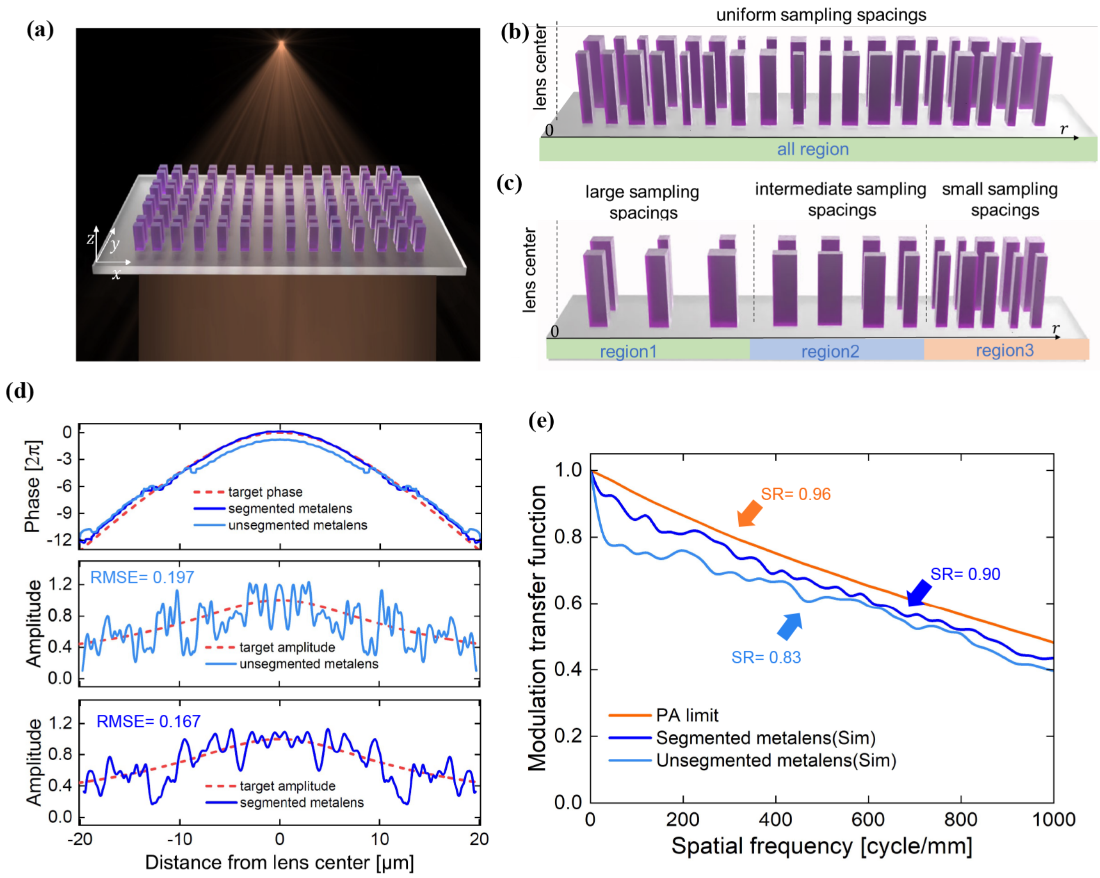

Figure 3. Design strategies and simulation results of the metalens with 0.9 NA. (a) Schematic diagram of a PA cylindrical metalens designed using interferometric unit cells. The y direction is periodic. Plane waves are incident from below and focus above the lens. (b) Schematic diagram of the unsegmented sampling principle with a uniform sampling period. (c) Schematic diagram of different areas with different sampling spacing. Adopting large, intermediate, and small sampling spacing from the center of the lens to the edge, they satisfy the Nyquist sampling theorem. Comparison of the phase, amplitude (d), and MTF (e) of PA metalenses built using unsegmented sampling and segmented sampling, respectively.

Information for the discussion about the material loss on the metalens performance).

Metalens with a Large NA and High MTF. We designed 0.9 NA cylindrical metalenses that focused incident TE-polarized light at a wavelength of 940 nm. Figure 3(a) shows a schematic of the PA cylindrical metalens. The first metalens was constructed using a universal discrete method (uniform sampling period), as shown in Figure 3(b). The period P_x of the interference unit cells in the x direction was set to 0.375 μm (the sampling spacing of the metalens was unsegmented). The unit cells' period P_y along the y axis was 0.92 μm (avoids diffraction order). The nanopillars' height h was 1.2 μm. We selected nanopillars in the single-mode region[44] that are weakly affected by adjacent structures to design the metalens. Please see the Methods section and Supporting Information for the details of the metalens design and simulation. Figure 3(d) shows the phase and amplitude (unsegmented) of the designed metalens. The actual amplitude oscillates with the target amplitude, and the actual phase has a certain deviation from the target phase. This amplitude oscillation and phase deviation mainly originate from the lens's small sampling spacing, causing near-field coupling of adjacent unit cells. Other factors like the refractive index and the geometric parameters of unit cells also contribute. Still, they are minor factors since we have already chosen a high refractive index material and single-mode nanopillars[44] to reduce the coupling caused by them. However, a small sampling spacing is a general measure since the amplitude and phase of lenses with large NA change quickly;[42,43] therefore, it is almost impossible to achieve a perfect target (e.g., nonoscillating amplitude) profile at large NA. Nevertheless, it is no matter since we found the oscillation impacts MTF, but the impact is not particularly serious. The support is that our PA metalens also achieved a simulated SR of 0.83, which exceeds the theoretical ideal SR of the PO lens.

To alleviate the amplitude oscillation and phase deviation issue and further improve the MTF of the PA metalens, we propose a segmented sampling principle, as shown in Figure 3(c), where the phase and amplitude near the center of the lens change slowly, using large-period unit cells, while the edge with rapidly changing amplitude and phase adopts small-period unit cells. We used three-segment sampling spacing of 0.45, 0.4, and 0.375 μm to redesign a 0.9 NA PA metalens, where the ratio of the three-segment lengths was 0.35:0.43:0.22 (see Supporting Information for selection of the basis of these parameters). The unit cells' period P_y along the y axis and height h remained unchanged. Figure 3(d) shows the amplitude and phase comparisons between segmented and unsegmented sampling. First of all, it is intuitive to see that the phase deviation of the segmented sampling metalens is smaller than that of the segmented sampling metalens. Then the root-mean-square error (RMSE)[45] was employed to calculate the absolute difference between the target amplitude and actual amplitude profiles. The segmented sampling metalens had a

https://doi.org/10.1021/acsphotonics.2c02029
ACS Photonics XXXX, XXX, XXX−XXX

lower RMSE; thus, its simulated amplitude was more consistent with the target. Further, Figure 3(e) demonstrates that the segmented metalens has a higher MTF than the unsegmented sampling one and the SR is enhanced from 0.83 to 0.9 using a segmented sampling method. Finally, our PA metalens with 0.9 NA achieves an SR of 0.9, which is 10% more than the 0.8 theoretical limit of the PO profile. In addition, we also evaluated the efficiency of PA and PO metalenses; our PA metalens achieves an efficiency of 80.1%, which is 7.6% more than the 72.5% theoretical limit of the PO profile (see the Supporting Information for detailed definition and analysis about the efficiency).

Note that the amplitude oscillating problem similarly exists in the PO metalens (the amplitude and phase are plotted in Figure S6 of the Supporting Information). In contrast, the amplitude of the PA metalens oscillates along with the target (SR = 0.90), whereas the amplitude of the PO metalens oscillates along with unity (SR = 0.68). The PA metalens had a higher MTF than that of the PO. In addition, the results in Figure 3(e) show that the effect of the oscillating amplitude on the SR of the metalens is slight and that the SR can be further enhanced by the segmented sampling principle, reducing coupling to approach the trend of the amplitude profile more closely.

We also designed several PA metalenses with NAs of 0.7, 0.8, and 0.85 and a series of PO metalenses with the same NAs. Please refer to Table S1 in the Supporting Information for the design details. The corresponding SRs are shown in Figure 4.

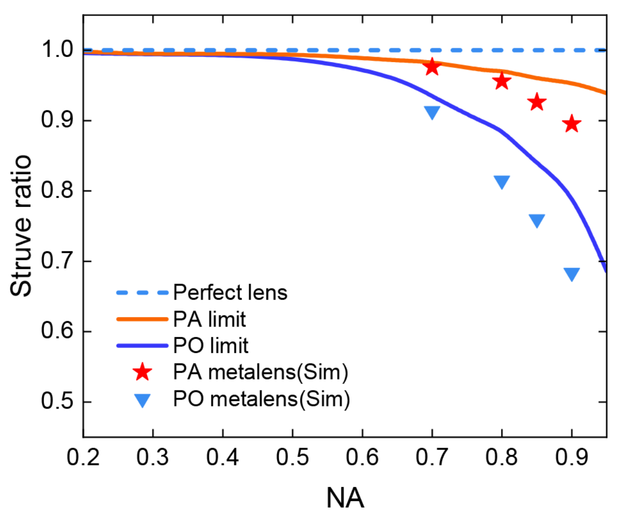

Figure 4. Summary SRs of PA and PO metalenses designed and simulated with various NAs.

The red star and blue triangle represent the SRs of the PA and PO metalenses, respectively. All PA metalens SRs were greater than 0.9. Although they are slightly lower than the PA limit (0.96), they are much higher than those of the PO metalens (0.68) and the theoretical upper limit (0.8) of the PO profile. Please refer to the Supporting Information for more simulation results for these metalenses.

Experiment on the Large-NA and High-MTF Metalens. To experimentally confirm the large NA metalens with a high MTF, we designed, fabricated, and characterized 240-μm-aperture PA cylindrical metalenses with an NA of 0.9. Note that for facilitating characterization, the metalens aperture in the experiment is larger than that in the previous simulation, which is a common treatment in articles about metalenses[26,46] (the small aperture is convenient for simulation, and the large aperture is suitable for characterization). However, the aperture difference does not affect the validation of metalens performance because the sampling principle (only related to NA) and design approach are the same. The metalenses were fabricated using standard electron-beam lithography and dry etching manufacturing techniques. Please refer to the Method section and the Supporting Information for the device fabrication process and process parameters. An optical microscope image of the fabricated PA cylindrical metalens is shown in Figure 5(a), wherein light is focused in a one-dimensional direction, and another direction is arranged periodically. Figure 5(b) shows scanning electron microscopy (SEM) images of the center of the PA metalens. The red dashed box indicates that the interferometric unit cell consisted of two hydrogenated silicon nanopillars in the magnified SEM image. The SEM tilted view in the inset shows nanostructures that exhibit good verticality and a high aspect ratio.

We built an experimental setup to characterize the proposed metamodel. The characterization details can be found in the Methods section and Supporting Information. The simulated and experimental PSFs of PA metalenses with an NA of 0.9 are shown in Figure 5(c). The distribution of the experimental PSF was the same as that in the simulation. The corresponding MTF, that is, the modulus of the Fourier transform of the PSF, was also calculated and plotted in Figure 5(d). The PA metalens achieved an experimental SR of 0.77, and the corresponding simulated SR was 0.89. The experimental MTF was slightly lower than the simulated result owing to the existing fabrication error. A similar problem exists in the fabricated PO metalens (the experimental results are provided in Supporting Information Figure S12). Despite this, the experimental SR of our PA metalens with a 0.9 NA is still 0.09 higher than the simulated SR (0.68) of the PO metalens. The results confirm that the MTF of a large-NA lens can be improved by approximately realizing the trend of the required amplitude.

■ CONCLUSION

In conclusion, we presented a simplified PA profile and revealed that the amplitude does not require perfect matching and that merely achieving the approximate trend is sufficient to increase the MTF of a large-NA lens. We used interferometric unit cells to modulate independently the amplitude and phase and applied a segmented sampling principle to alleviate the coupling to design a series of metalenses with NAs from 0.7 to 0.9 under TE-polarized light at a 940 nm wavelength. All of these metalenses achieved a simulated SR higher than 0.9. We also fabricated a 0.9 NA metalens and demonstrated an experimental SR exceeding 0.77. The results confirm our insights and the breakthrough in the design of metalenses using the PA profile. Our approach for designing large-NA metalenses is general and extensible, unlike topology optimization, which is limited by the device size owing to excessive demand on computing resources. Our approach can also extend to normal rotational symmetric metalenses, but more efficient and small dimension unit cells for amplitude and phase modulation will be required. There are possible ways to find these unit-cell structures, such as through deep neural networks.[47] In addition, the amplitude modulation term of the PA profile is only position-dependent and wavelength-independent, which is promising for future generalization of

https://doi.org/10.1021/acsphotonics.2c02029
ACS Photonics XXXX, XXX, XXX−XXX

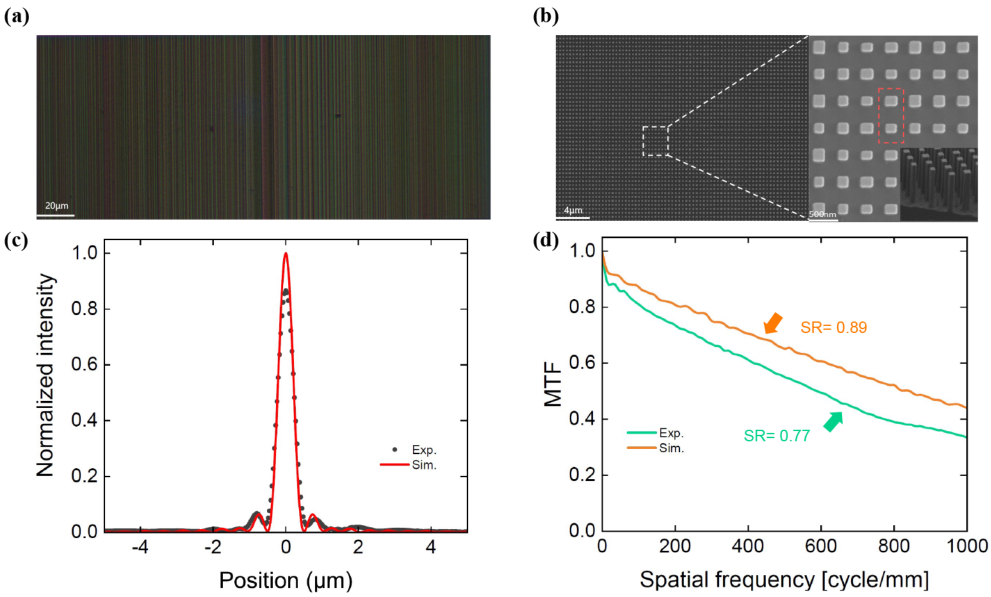

Figure 5. Experimental results for the high-MTF metalens with a 0.9 NA. (a) Optical microscope image of the fabricated PA cylindrical metalens. The scale bar is 20 μm. (b) Scanning electron micrographs (SEMs) of the PA metalens are shown in the left side. The scale bar is 4 μm. The right side is a zoomed-in SEM image corresponding to the white dashed box region. The scale bar is 500 nm. An interferometric unit-cell structure of the metalens is indicated by the red dashed box. The inset is a SEM tilted view. (c) Simulated and experimental PSFs of the PA metalens. (d) MTFs of the fabricated PA metalens, along with their simulated values.

our approach to broadband achromatic metalenses with high MTFs and high performance. Our work provides a paradigm for designing large-NA metalenses with high MTF. It is expected to promote high-resolution imaging applications and the development of metalenses with large NA for advanced optical systems.

■ METHOD

Design and Simulation. The PA metalens was designed by establishing an interferometric unit cell library. We calculated the required amplitude and phase at each location based on the optical parameters of the metalens and segmented sampling principle. Next, we swept the different substructures' length and width (l, w) using rigorous coupled-wave analysis (RCWA). According to eq 2, we selected high-transmittance nanopillars to establish the interferometric unit-cell library. Note that for unit cells with large deviations from the target value, particle swarm optimization (PSO)[48] and Reticolo (an RCWA solver)[49] were used to assist in the redesign (small periods are more difficult to design directly, and optimization is required). Finally, using the established library, we selected the base unit cells that met the amplitude and phase requirements at each position and combined them into a metalens. The entire metalens was simulated using commercial Lumerical FDTD software. The phase and amplitude of the metalens were obtained from the electric field E_y at the output planes of the metalens, where the phase and amplitude were the angle and modulus of E_y, respectively. Note that the amplitude was averaged according to the base unit-cell periods. The PSF of the metalens was the electric energy density distribution at the focal plane, and the MTF was the modulus of the Fourier transform.

Fabrication. The fabrication tolerance of the critical dimension bias of the metalens is within ±5% (see Supporting Information for fabrication errors analysis). The metalens was fabricated on a 1-mm-thick glass substrate. A 1200-nm-thick layer of Si:H was deposited on the substrate using magnetron sputtering deposition (NSC-15, Optorun), similarly to the work in ref 41. Then, the substrate was spin-coated with a photoresist (ZEP520) and baked using thermal evaporation. Next, the metalens was patterned in the photoresist via an electron-beam lithography (EBPG5200, Raith) system. Next, the sample was developed in a mixed solution of pentyl acetate and isopropanol (IPA). Finally, inductively coupled plasma (ICP-RIE) etching with a mixture of SF_6 and CHF_3 was applied to etch the Si:H film using Oxford PlasmaPro 100 Cobra 300. Additional details and process parameters are provided in the Supporting Information.

Characterization. To estimate the MTF and SR of the metalens, we used an experimental setup similar to those described in the literature.[26,50] The schematic and actual photo of the setup are shown in Figure S11. A plano-convex lens was used to collimate the fiber-coupled light source. The collimated light beam was filtered using a bandpass filter and polarized using a linear polarizer. Then, the beam was normally directed and focused on the metalens. Next, the focal plane was imaged onto a CMOS detector using a 0.95 NA 100× objective (Olympus PlanFLN100X) and an 80 mm focal length tube lens. The PSF was obtained using a line scan of the focal plane image, and the MTF was determined from the PSF. The SR was calculated according to the definition provided in the Supporting Information. Additional characterization details are provided in the Supporting Information.

■ ASSOCIATED CONTENT

Supporting Information

The Supporting Information is available free of charge at https://pubs.acs.org/doi/10.1021/acsphotonics.2c02029.

Detailed definition of Struve ratio, calculation of MTFs by angular spectrum theory, additional examples of independent modulation of phase and amplitude, segmented sampling details, evaluating the effect of the

https://doi.org/10.1021/acsphotonics.2c02029
ACS Photonics XXXX, XXX, XXX−XXX

material loss, fabrication errors and efficiency analysis, full-wave simulation results, the procedures of fabrication and characterization, more experimental results, and supplementary references (PDF)

AUTHOR INFORMATION

Corresponding Authors

Xiong Dun − *Institute of Precision Optical Engineering, School of Physics Science and Engineering, Tongji University, Shanghai 200092, China; MOE Key Laboratory of Advanced Micro-Structured Materials, Shanghai 200092, China; Shanghai Frontiers Science Center of Digital Optics, Shanghai 200092, China*; Email: dunx@tongji.edu.cn

Xinbin Cheng − *Institute of Precision Optical Engineering, School of Physics Science and Engineering and Shanghai Institute of Intelligent Science and Technology, Tongji University, Shanghai 200092, China; MOE Key Laboratory of Advanced Micro-Structured Materials, Shanghai 200092, China; Shanghai Frontiers Science Center of Digital Optics, Shanghai 200092, China*; orcid.org/0000-0002-3855-483X; Email: chengxb@tongji.edu.cn

Authors

Jian Zhang − *Institute of Precision Optical Engineering, School of Physics Science and Engineering, Tongji University, Shanghai 200092, China; MOE Key Laboratory of Advanced Micro-Structured Materials, Shanghai 200092, China; Shanghai Frontiers Science Center of Digital Optics, Shanghai 200092, China*

Jingyuan Zhu − *Institute of Precision Optical Engineering, School of Physics Science and Engineering, Tongji University, Shanghai 200092, China; MOE Key Laboratory of Advanced Micro-Structured Materials, Shanghai 200092, China; Shanghai Frontiers Science Center of Digital Optics, Shanghai 200092, China*

Zhanyi Zhang − *Institute of Precision Optical Engineering, School of Physics Science and Engineering and Shanghai Institute of Intelligent Science and Technology, Tongji University, Shanghai 200092, China; MOE Key Laboratory of Advanced Micro-Structured Materials, Shanghai 200092, China; Shanghai Frontiers Science Center of Digital Optics, Shanghai 200092, China*

Chao Feng − *Institute of Precision Optical Engineering, School of Physics Science and Engineering, Tongji University, Shanghai 200092, China; MOE Key Laboratory of Advanced Micro-Structured Materials, Shanghai 200092, China; Shanghai Frontiers Science Center of Digital Optics, Shanghai 200092, China*

Zhanshan Wang − *Institute of Precision Optical Engineering, School of Physics Science and Engineering and Shanghai Institute of Intelligent Science and Technology, Tongji University, Shanghai 200092, China; MOE Key Laboratory of Advanced Micro-Structured Materials, Shanghai 200092, China; Shanghai Frontiers Science Center of Digital Optics, Shanghai 200092, China*

Wolfgang Heidrich − *Visual Computing Center, King Abdullah University of Science and Technology, Thuwal 23955-6900, Kingdom of Saudi Arabia*

Complete contact information is available at:
https://pubs.acs.org/10.1021/acsphotonics.2c02029

Author Contributions

J.Z. and X.D. contributed equally to this work.

Funding

This work was supported by Shanghai Pujiang Program (20PJ1414200); National Natural Science Foundation of China (61621001, 61925504, 6201101335, 62020106009, 62105243, 62192770, 62192772); Science and Technology Commission of Shanghai Municipality (17JC1400800, 20JC1414600, 21JC1406100); and the Fundamental Research Funds for the Central Universities and the Shanghai Municipal Science and Technology Major Project (2021SHZDZX0100).

Notes

The authors declare no competing financial interest.

REFERENCES

(1) Sheppard, C. J. Cylindrical lenses—focusing and imaging: a review. *Applied optics* **2013**, *52*, 538−545.

(2) Zhang, Y.; Gross, H. Systematic design of microscope objectives. Part I: System review and analysis. *Advanced Optical Technologies* **2019**, *8*, 313−347.

(3) Chun, W.; Do, D.; Gweon, D.-G. Design and demonstration of multimodal optical scanning microscopy for confocal and two-photon imaging. *Rev. Sci. Instrum.* **2013**, *84*, 013701.

(4) Fischer, R.; Tadic-Galeb, B.; Yoder, P. *Optical System Design*; McGraw-Hill Education, 2008.

(5) Born, M.; Wolf, E. *Principles of Optics*; Cambridge University Press, Cambridge, U.K., 1999.

(6) Boreman, G. D. *Modulation Transfer Function in Optical and Electro-Optical Systems*; SPIE Press: Bellingham, WA, 2001; Vol. *4*.

(7) Engelberg, J.; Levy, U. Standardizing flat lens characterization. *Nat. Photonics* **2022**, *16*, 171−173.

(8) Estakhri, N. M.; Alu, A. Wave-front transformation with gradient metasurfaces. *Physical Review X* **2016**, *6*, 041008.

(9) Sang, D.; Xu, M.; Pu, M.; Zhang, F.; Guo, Y.; Li, X.; Ma, X.; Fu, Y.; Luo, X. Toward High-Efficiency Ultrahigh Numerical Aperture Freeform Metalens: From Vector Diffraction Theory to Topology Optimization. *Laser & Photonics Reviews* **2022**, *16*, 2200265.

(10) Dun, X.; Ikoma, H.; Wetzstein, G.; Wang, Z.; Cheng, X.; Peng, Y. Learned rotationally symmetric diffractive achromat for full-spectrum computational imaging. *Optica* **2020**, *7*, 913−922.

(11) Wang, P.; Mohammad, N.; Menon, R. Chromatic-aberration-corrected diffractive lenses for ultra-broadband focusing. *Sci. Rep.* **2016**, *6*, 1−7.

(12) Banerji, S.; Meem, M.; Majumder, A.; Vasquez, F. G.; Sensale-Rodriguez, B.; Menon, R. Imaging with flat optics: metalenses or diffractive lenses? *Optica* **2019**, *6*, 805−810.

(13) Moshfeghi, M. Sidelobe suppression in annular array and axicon imaging systems. *J. Acoust. Soc. Am.* **1988**, *83*, 2202−2209.

(14) Reddy, A.; Hashemi, M. Apodization pupils: design and performance. *Journal of Physics: Conference Series* **2018**, *1096*, 012140.

(15) Yu, N.; Genevet, P.; Kats, M. A.; Aieta, F.; Tetienne, J.-P.; Capasso, F.; Gaburro, Z. Light propagation with phase discontinuities: generalized laws of reflection and refraction. *Science* **2011**, *334*, 333−337.

(16) Kildishev, A. V.; Boltasseva, A.; Shalaev, V. M. Planar photonics with metasurfaces. *Science* **2013**, *339*, 1232009.

(17) Yu, N.; Capasso, F. Flat optics with designer metasurfaces. *Nat. Mater.* **2014**, *13*, 139−150.

(18) Yang, Z.; Wang, Z.; Wang, Y.; Feng, X.; Zhao, M.; Wan, Z.; Zhu, L.; Liu, J.; Huang, Y.; Xia, J.; et al. Generalized Hartmann-Shack array of dielectric metalens sub-arrays for polarimetric beam profiling. *Nat. Commun.* **2018**, *9*, 1−7.

(19) Shi, Y.; Song, Q.; Toftul, I.; Zhu, T.; Yu, Y.; Zhu, W.; Tsai, D. P.; Kivshar, Y.; Liu, A. Q. Optical manipulation with metamaterial structures. *Applied Physics Reviews* **2022**, *9*, 031303.

(20) Wang, Y.; Chen, Q.; Yang, W.; Ji, Z.; Jin, L.; Ma, X.; Song, Q.; Boltasseva, A.; Han, J.; Shalaev, V. M.; et al. High-efficiency

broadband achromatic metalens for near-IR biological imaging window. *Nat. Commun.* **2021**, *12*, 1−7.

(21) Khorasaninejad, M.; Chen, W. T.; Devlin, R. C.; Oh, J.; Zhu, A. Y.; Capasso, F. Metalenses at visible wavelengths: Diffraction-limited focusing and subwavelength resolution imaging. *Science* **2016**, *352*, 1190−1194.

(22) Khorasaninejad, M.; Zhu, A. Y.; Roques-Carmes, C.; Chen, W. T.; Oh, J.; Mishra, I.; Devlin, R. C.; Capasso, F. Polarization-insensitive metalenses at visible wavelengths. *Nano Lett.* **2016**, *16*, 7229−7234.

(23) Paniagua-Dominguez, R.; Yu, Y. F.; Khaidarov, E.; Choi, S.; Leong, V.; Bakker, R. M.; Liang, X.; Fu, Y. H.; Valuckas, V.; Krivitsky, L. A.; et al. A metalens with a near-unity numerical aperture. *Nano Lett.* **2018**, *18*, 2124−2132.

(24) Byrnes, S. J.; Lenef, A.; Aieta, F.; Capasso, F. Designing large, high-efficiency, high-numerical-aperture, transmissive meta-lenses for visible light. *Opt. Express* **2016**, *24*, 5110−5124.

(25) Arbabi, A.; Arbabi, E.; Mansouree, M.; Han, S.; Kamali, S. M.; Horie, Y.; Faraon, A. Increasing efficiency of high numerical aperture metasurfaces using the grating averaging technique. *Sci. Rep.* **2020**, *10*, 1−10.

(26) Phan, T.; Sell, D.; Wang, E. W.; Doshay, S.; Edee, K.; Yang, J.; Fan, J. A. High-efficiency, large-area, topology-optimized metasurfaces. *Light: Sci. Applications* **2019**, *8*, 1−9.

(27) Plidschun, M.; Ren, H.; Kim, J.; Förster, R.; Maier, S. A.; Schmidt, M. A. Ultrahigh numerical aperture meta-fibre for flexible optical trapping. *Light: Sci. Applications* **2021**, *10*, 1−11.

(28) Aieta, F.; Genevet, P.; Kats, M. A.; Yu, N.; Blanchard, R.; Gaburro, Z.; Capasso, F. Aberration-free ultrathin flat lenses and axicons at telecom wavelengths based on plasmonic metasurfaces. *Nano Lett.* **2012**, *12*, 4932−4936.

(29) Cai, H.; Srinivasan, S.; Czaplewski, D. A.; Martinson, A. B.; Gosztola, D. J.; Stan, L.; Loeffler, T.; Sankaranarayanan, S. K.; López, D. Inverse design of metasurfaces with non-local interactions. *npj Computational Materials* **2020**, *6*, 1−8.

(30) Chung, H.; Miller, O. D. High-NA achromatic metalenses by inverse design. *Opt. Express* **2020**, *28*, 6945−6965.

(31) Mansouree, M.; Kwon, H.; Arbabi, E.; McClung, A.; Faraon, A.; Arbabi, A. Multifunctional 2.5 D metastructures enabled by adjoint optimization. *Optica* **2020**, *7*, 77−84.

(32) Balanis, C. A. *Advanced Engineering Electromagnetics*; John Wiley & Sons, 1999.

(33) Goodman, J. W. *Introduction to Fourier Optics*, 3rd ed.; Roberts and Company Publishers, 2005; Vol. 3.

(34) Overvig, A. C.; Shrestha, S.; Malek, S. C.; Lu, M.; Stein, A.; Zheng, C.; Yu, N. Dielectric metasurfaces for complete and independent control of the optical amplitude and phase. *Light: Science & Applications* **2019**, *8*, 92.

(35) Liu, W.; Li, Z.; Li, Z.; Cheng, H.; Tang, C.; Li, J.; Chen, S.; Tian, J. Energy-tailorable spin-selective multifunctional metasurfaces with full Fourier components. *Adv. Mater.* **2019**, *31*, 1901729.

(36) Ren, H.; Fang, X.; Jang, J.; Bürger, J.; Rho, J.; Maier, S. A. Complex-amplitude metasurface-based orbital angular momentum holography in momentum space. *Nat. Nanotechnol.* **2020**, *15*, 948−955.

(37) Fan, Q.; Liu, M.; Zhang, C.; Zhu, W.; Wang, Y.; Lin, P.; Yan, F.; Chen, L.; Lezec, H. J.; Lu, Y.; et al. Independent amplitude control of arbitrary orthogonal states of polarization via dielectric metasurfaces. *Phys. Rev. Lett.* **2020**, *125*, 267402.

(38) Wu, T.; Zhang, X.; Xu, Q.; Plum, E.; Chen, K.; Xu, Y.; Lu, Y.; Zhang, H.; Zhang, Z.; Chen, X.; et al. Dielectric metasurfaces for complete control of phase, amplitude, and polarization. *Advanced Optical Materials* **2022**, *10*, 2101223.

(39) Zheng, C.; Li, J.; Yue, Z.; Li, J.; Liu, J.; Wang, G.; Wang, S.; Zhang, Y.; Zhang, Y.; Yao, J. All-dielectric trifunctional metasurface capable of independent amplitude and phase modulation. *Laser & Photonics Reviews* **2022**, *16*, 2200051.

(40) Liu, M.; Zhu, W.; Huo, P.; Feng, L.; Song, M.; Zhang, C.; Chen, L.; Lezec, H. J.; Lu, Y.; Agrawal, A.; et al. Multifunctional metasurfaces enabled by simultaneous and independent control of phase and amplitude for orthogonal polarization states. *Light: Science & Applications* **2021**, *10*, 107.

(41) He, T.; Zhang, J.; Jiao, H.; Wang, Z.; Cheng, X. Near-infrared broadband Si:H/SiO2 multilayer gratings with high tolerance to fabrication errors. *Nanotechnology* **2020**, *31*, 315203.

(42) Liang, H.; Martins, A.; Borges, B.-H. V.; Zhou, J.; Martins, E. R.; Li, J.; Krauss, T. F. High performance metalenses: numerical aperture, aberrations, chromaticity, and trade-offs. *Optica* **2019**, *6*, 1461−1470.

(43) Lalanne, P.; Chavel, P. Metalenses at visible wavelengths: past, present, perspectives. *Laser Photonics Reviews* **2017**, *11*, 1600295.

(44) Matsui, T.; Iizuka, H. Effect of finite number of nanoblocks in metasurface lens design from bloch-mode perspective and its experimental verification. *ACS Photonics* **2020**, *7*, 3448−3455.

(45) Sun, Y.; Wang, C.; Zheng, S.; Tao, X.; Liu, X.; Li, Y.; Wu, F.; Zheng, Z. Double-layer polarization-independent achromatic metasurface array for optical fiber bundle coupling in microendoscope. *Sci. Rep.* **2022**, *12*, 1−11.

(46) Chen, W. T.; Zhu, A. Y.; Sanjeev, V.; Khorasaninejad, M.; Shi, Z.; Lee, E.; Capasso, F. A broadband achromatic metalens for focusing and imaging in the visible. *Nature Nanotechnol.* **2018**, *13*, 220−226.

(47) An, S.; Zheng, B.; Shalaginov, M. Y.; Tang, H.; Li, H.; Zhou, L.; Ding, J.; Agarwal, A. M.; Rivero-Baleine, C.; Kang, M.; et al. A freeform dielectric metasurface modeling approach based on deep neural networks. 2020−01−01. *arXiv (physics.optics)*, arXiv:2001.00121 (accessed 2021−05−12).

(48) Kennedy, J.; Eberhart, R. Particle swarm optimization. *Proceedings of ICNN'95-international conference on neural networks*; 1995; pp 1942−1948.

(49) Hugonin, J. P.; Lalanne, P. Reticolo software for grating analysis. 2021−01−04. *arXiv (physics.optics)*, arXiv:2101.00901 (accessed 2021−02−08).

(50) Engelberg, J.; Zhou, C.; Mazurski, N.; Bar-David, J.; Kristensen, A.; Levy, U. Near-IR wide-field-of-view Huygens metalens for outdoor imaging applications. *Nanophotonics* **2020**, *9*, 361−370.

https://doi.org/10.1021/acsphotonics.2c02029
ACS Photonics XXXX, XXX, XXX−XXX